A DPG method for planar div-curl problems

Jiaqi Li, Leszek Demkowicz

Oden Institute for Computational Engineering and Sciences

Abstract

The div-curl system arises in many fields including electromagnetism and fluid dynamics. We are particularly interested in the div-curl problem in 2D multiply-connected domains, as a simplified model of flow around airfoils. In such domains, well-posedness of the problem depends on the prescription of additional line integrals (circulation), apart from standard boundary conditions. We apply the DPG method to the ultraweak formulation of the problem and impose the circulation condition in a constrained minimization framework, which results in a mixed problem. We prove the discrete stability with Brezzi's theory and demonstrate convergence with numerical experiments in a toroidal domain. We also perform h-adaptive refinements based on the DPG a posteriori error estimator.

1 Introduction

The Discontinuous Petrov-Galerkin (DPG) method is a novel finite element technique and has been developing rapidly in recent years [15, 16]. It admits the interpretation of a minimum-residual method, where the residual is measured in a dual norm [29, 27]. In Hilbert spaces, the dual norm can be computed with the introduction of a Riesz map, and the DPG method reduces to a weighted least-squares finite element method [26]. Consequently, the DPG method comes with many desirable properties: a symmetric positive-definite stiffness matrix, discrete stability (inf-sup condition), and a posteriori error estimates [11].

The applications of DPG are diverse. Examples include convection-dominated diffusion [13, 28], Stokes problem [35], linear elasticity [25], time-harmonic wave propogation [33], incompressible Navier-Stokes equations [36], and viscous compressible flows [12, 34].

In this paper, we propose a DPG method for planar div-curl problems. The div-curl system arises in many fields including electromagenetism and fluid dynamics. Moreover, we are particularly interested in div-curl problems in 2D multiply-connected domains, as a simplified model of flow around airfoils (see Fig. 1). This model neglects viscosity and compressibility; it is relevant when we are concerned with the lift on slender bodies (e.g., airfoils) with a small angle of attack and a low inflow Mach number [1].

Planar div-curl problem. Consider a domain $\Omega \subset \mathbb{R}^2$ with boundary $\Gamma := \partial\Omega$, and a vector field $\boldsymbol{u} : \overline{\Omega} \to \mathbb{R}^2$ satisfying

$$\operatorname{div} \boldsymbol{u} = f \quad \text{in } \Omega, \tag{1a}$$

$$\operatorname{curl} \boldsymbol{u} = g \quad \text{in } \Omega, \tag{1b}$$

$$\boldsymbol{u} \cdot \boldsymbol{n} = \mu \quad \text{on } \Gamma, \tag{1c}$$

where $\operatorname{curl} \boldsymbol{u} := u_{2,1} - u_{1,2}$ is the scalar curl of a 2D vector field. Ω is assumed to have piecewise $C^{1,1}$ boundary so that the normal trace exists everywhere except for corners. We further assume that

$$\int_\Omega f = \int_\Gamma \mu.$$

The unknown vector field $\boldsymbol{u}$ represents fluid velocity for the flow problem in mind.

According to Auchmuty and Alexander [3], this problem is well posed for simply-connected domains; but in multiply-connected domains, there is a finite-dimensional family of solutions to problem (1). The dimension of the solution space is the Betti number of the domain, i.e., number of holes. The problem is well-posed with a unique solution only when certain line integrals are further prescribed. To make things specific, we focus on a doubly-connected domain, e.g., flow around an airfoil (see Fig. 1). One line integral has to be specified. In aerodynamics this is known as "circulation condition"—we need to prescribe the circulation along a closed curve that encloses the airfoil. One possible choice is to prescribe the line integral around the boundary of the airfoil, i.e.,

$$\int_{\Gamma_1} u_t \, ds = \kappa \tag{2}$$

for some constant κ. Here Γ_1 represents the airfoil boundary, and on Γ_1 the velocity satisfies the no-penetration condition $\boldsymbol{u} \cdot \boldsymbol{n} = 0$. Γ_0 is the outer boundary, which is sufficiently far from the airfoil such that we can prescribe the flux condition $\boldsymbol{u} \cdot \boldsymbol{n} = \boldsymbol{u}_\infty \cdot \boldsymbol{n}$ on Γ_0. It is equivalent to set $\mu = 0$ on Γ_0 and $\mu = \boldsymbol{u}_\infty \cdot \boldsymbol{n}$ on Γ_1 in (1c). In this article, we will mainly focus on the div-curl problem with normal boundary conditions (1) and the additional circulation condition (2), although we remark that the proposed DPG framework is fully general and can be applied to div-curl problems with other types of boundary conditions and prescribed line integrals.

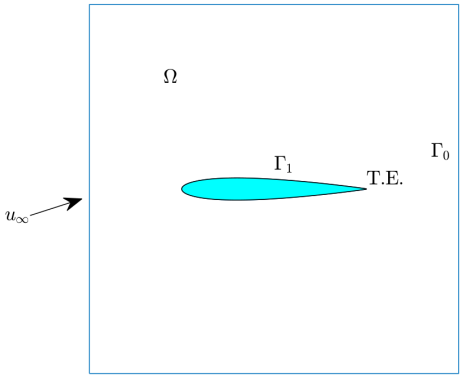

Figure 1: Flow around an airfoil.

Remark. The idea of DPG with constraints can be first found in the work of Ellis et al. [19]. But the reasons for imposing constraints are different. Ellis et al. impose constraints to ensure mass conservation, while we have to prescribe circulation (2) to guarantee well-posedness.

Numerical algorithms for div-curl problems abound in literature. Nicolaides [30] proposed a control volume method for planar div-curl systems based on dual pairs of meshes (Voronoi-Delaunay mesh pairs)

and later extended it to 3D with Wu [31]. However, this method is in general first order only. Hyman and Shashkov [24] constructed mimetic finite difference methods for Maxwell equations on 2D rectangular grids.

As for finite element methods, we first note that standard conforming least-squares finite element methods fail in nonsmooth or nonconvex domains Ω (e.g., the domain shown in Fig. 1) [7]. A finite element subspace of $H(\text{curl}, \Omega)$ and $H(\text{div}, \Omega)$ must be both tangentially and normally continuous across element interfaces. Hence the basis functions are continuous and in $\boldsymbol{H}^1(\Omega) := [H^1(\Omega)]^N, N = 2, 3$. However, as shown by Costabel [14], unless Ω has a smooth boundary or is a convex polyhedron, $H_0(\text{div}, \Omega) \cap \boldsymbol{H}^1(\Omega)$ is a closed proper subspace of $H_0(\text{div}, \Omega) \cap H(\text{curl}, \Omega)$. Thus C^0 elements do not have the approximability property; see Corollary 2.30, p.97 in [20]. To overcome this issue, Bensow and Larson [6] developed a discontinuous least-squares finite element method for the div-curl problem, where discontinuous elements enables convergence for less regular data and in nonconvex domains. The tangential and normal continuity, as well as boundary conditions, are weakly enforced through the least-squares functional. Bochev et al. [7], on the other hand, employed either $H(\text{curl})$- or $H(\text{div})$- conforming spaces, and defined a discrete divergence/curl operator to complete computation of the residual. In [9], Cao et al. presented a new primal-dual weak Galerkin method to solve div-curl systems. Their method is based on a weak formulation that relaxes both (1a) and (1b) and invokes discrete weak gradient and curl operator defined in a similar way as [7]. With discontinuous elements, they are able to approximate low H^α-regularity ($\alpha \geq 0$) solution.

The DPG method we propose shares the same benefit: it is based on the ultraweak formulation, obtained by relaxing both (1a) and (1b); consequently, the solution is only assumed to be in $\boldsymbol{L}^2(\Omega)$. With discontinuous piecewise polynomials to discretize $\boldsymbol{L}^2(\Omega)$, approximability is not an issue. We demonstrated the ability of our method to capture solution with low regularity by solving the same problem with singular solutions as [9]; but in contrast, the DPG solution displays stability from day one, and converges not just asymptotically, but from the beginning (on a very coarse mesh), at the optimal rate. The built-in a posteriori error estimator in DPG also allows us to perform adaptive refinements, which is particularly important in the case of singular problems. Another feature of our method is the mathematically rigorous treatment of the circulation condition, which makes it possible to deal with multiply-connected domains and get convergent solutions in $\boldsymbol{L}^2(\Omega)$, not just in the quotient space.

This paper is structured as follows: In Section 2, we describe the ultraweak variational formulation of the div-curl system with normal boundary conditions (1), as well as the DPG discretization techniques. This is relevant when the domain is simply-connected and act as a stepping stone to our algorithms for multiply-connected domains. Then we study the L^2 adjoint operator (used in the ultraweak formulation) within a closed operator framework in Section 3. In Section 4, we present a constrained minimization framework to impose the circulation constraint (2), and prove the well-posedness of the resulting mixed problem. Section 5 is devoted to numerical experiments. Finally, in Section 6, we summarize our findings and point out future directions.

2 Ultraweak variational formulation and DPG discretization

2.1 DPG method in a nutshell

Consider an abstract variational problem

$$\begin{cases} \text{Find } u \in \mathcal{U} : \\ Bu = l \quad \text{in } \mathcal{V}', \end{cases}$$

where $\mathcal{U}$ and $\mathcal{V}$ are Hilbert spaces, $B : \mathcal{U} \to \mathcal{V}'$ is a bounded linear operator, which is dictated by the problem under consideration, and $l \in \mathcal{V}'$ is the load. Suppose the variational problem specifies a bilinear form $b : \mathcal{U} \times \mathcal{V} \to \mathbb{R}$; then B is defined by

$$\langle Bw, v \rangle := b(w, v)$$

where $\langle \cdot, \cdot \rangle$ represents the duality pairing between $\mathcal{V}'$ and $\mathcal{V}$. Henceforth, we use the same bracket symbol to denote duality pairings, and the underlying spaces should be clear from the context. Given a discrete trial space $\mathcal{U}_h \subset \mathcal{U}$, the *ideal* DPG method solves the minimum-residual problem:

$$\begin{cases} \text{Find } u_h \in \mathcal{U}_h : \\ u_h = \underset{w_h \in U_h}{\arg\min} \|l - Bw_h\|_{\mathcal{V}'} \end{cases} \tag{3}$$

By introducing the Riesz map $R_{\mathcal{V}} : \mathcal{V} \to \mathcal{V}'$, the dual norm of the residual can be expressed as:

$$\|l - Bw_h\|_{\mathcal{V}'}^2 = \langle R_{\mathcal{V}}^{-1}(l - Bw_h), l - Bw_h \rangle.$$

Vanishing of the Gâteaux derivative at the minimzer u_h implies:

$$\langle R_{\mathcal{V}}^{-1} Bu_h, Bw_h \rangle = \langle R_{\mathcal{V}}^{-1} l, Bw_h \rangle \quad \forall w_h \in \mathcal{U}_h. \tag{4}$$

Or equivalently,

$$\langle B' R_{\mathcal{V}}^{-1} Bu_h, w_h \rangle = \langle B' R_{\mathcal{V}}^{-1} l, w_h \rangle \quad \forall w_h \in \mathcal{U}_h, \tag{5}$$

where $B' : \mathcal{V} \to \mathcal{U}'$ is the transpose of B. Equation (5) has the same structure as a standard Galerkin formulation, and can be incorporated into a standard finite element code.

If we introduce the error representation function $\psi := R_{\mathcal{V}}^{-1}(l - Bw_h)$, the residual minimization problem can be rewritten as a mixed problem:

$$\begin{cases} \text{Find } u_h \in \mathcal{U}_h, \psi \in \mathcal{V} : \\ (\psi, v)_{\mathcal{V}} + b(u_h, v) = l(v) \quad \forall v \in \mathcal{V}, \\ b(w_h, \psi) \qquad\qquad = 0 \qquad \forall w_h \in \mathcal{U}_h \end{cases} \tag{6}$$

where $(\cdot, \cdot)_{\mathcal{V}}$ denotes inner product on $\mathcal{V}$. The first equation in (6) follows from the definition of ψ, and the second equation is the vanishing of the Gâteaux derivative condition.

Practical DPG method. The only remaining problem with solving (5) or (6) is the inversion of Riesz operator $R_{\mathcal{V}}$. To perform actual computation, we use a discrete test space $\mathcal{V}_h \subset \mathcal{V}$ instead of $\mathcal{V}$. The fully discrete mixed problem now reads:

$$\begin{cases} \text{Find } u_h \in \mathcal{U}_h, \psi_h \in \mathcal{V}_h : \\ (\psi_h, v_h)_{\mathcal{V}} + b(u_h, v_h) = l(v_h) \quad \forall v_h \in \mathcal{V}_h, \\ b(w_h, \psi_h) \qquad\qquad = 0 \qquad \forall w_h \in \mathcal{U}_h. \end{cases} \tag{7}$$

For detailed analysis of the practical DPG method, we refer to [23] and comment that in practice, if we use elements of order p for $\mathcal{U}_h$, it suffices to use elements of order $p + \Delta p$ for $\mathcal{V}_h$ to guarantee stability. The details of discretization are postponed until Section 2.3.

2.2 Ultraweak variational formulation

After outlining the DPG framework, it remains to specify the variational formulation, i.e., $b(\cdot, \cdot)$. We choose to work with the ultraweak variational formulation and its broken counterpart, which constitutes the subject of this and next subsection. As detailed in [18], the relation between a closed operator A and its adjoint A^*,

$$(A\boldsymbol{u}, \boldsymbol{v}) = (\boldsymbol{u}, A^*\boldsymbol{v})$$

allows the introduction of the *ultraweak varational formulation*. Here $(\cdot, \cdot)$ denotes L^2 inner product. For the div-curl problem, $A\boldsymbol{u} := \begin{pmatrix} \operatorname{div} \boldsymbol{u} \\ \operatorname{curl} \boldsymbol{u} \end{pmatrix}$. To derive the L^2 adjoint, we multiply equation (1a) by v_1, (1b) by v_2, integrate by parts, and we get

$$\begin{aligned} -(\boldsymbol{u}, \nabla v_1) + \langle u_n, v_1 \rangle_\Gamma &= (f, v_1), \\ (\boldsymbol{u}, \nabla \times v_2) + \langle u_t, v_2 \rangle_\Gamma &= (g, v_2), \end{aligned}$$

where $\nabla \times w := w_{,2}\boldsymbol{e}_1 - w_{,1}\boldsymbol{e}_2$ is the vector curl of a scalar field, w, $(\cdot, \cdot)$ is the standard L^2 inner product on Ω, and $\langle \cdot, \cdot \rangle_\Gamma$ represents the duality pairing between $H^{-1/2}(\Gamma)$ and $H^{1/2}(\Gamma)$. The normal boundary condition (1c) translates into $u_n = \mu$, and we can get rid of the u_t term by testing with $v_2 \in H_0^1(\Omega)$. In the ultraweak variational formulation, we seek $\boldsymbol{u} \in \boldsymbol{L}^2(\Omega) := [L^2(\Omega)]^2$ satisfying

$$-(\boldsymbol{u}, \nabla v_1) = (f, v_1) - \langle \mu, v_1 \rangle_\Gamma \quad \forall v_1 \in H^1(\Omega), \tag{8a}$$

$$(\boldsymbol{u}, \nabla \times v_2) = (g, v_2) \qquad\qquad \forall v_2 \in H_0^1(\Omega). \tag{8b}$$

Therefore, formally $A^*\boldsymbol{v} := -\nabla v_1 + \nabla \times v_2$, and

$$b(\boldsymbol{u}, \boldsymbol{v}) := (\boldsymbol{u}, A^*\boldsymbol{v}) = (\boldsymbol{u}, -\nabla v_1 + \nabla \times v_2).$$

We equip the test space with quasi-optimal test graph norm [37]:

$$\|\boldsymbol{v}\|_{\mathcal{V}}^2 := \|\boldsymbol{v}\|^2 + \|A^*\boldsymbol{v}\|^2 = \|\boldsymbol{v}\|_{\boldsymbol{H}^1(\Omega)}^2 \tag{9}$$

where $\|\cdot\|$ denotes standard L^2 norm and $\boldsymbol{H}^1(\Omega) := [H^1(\Omega)]^2$. Using Closed Range Theorem [18], we can show that the well-posedness of (8) is equivalent to that of the primal problem (1), whose well-posedness has in turn been studied in [3, 2]. The full analysis is presented in Section 3 and 4.

2.3 Broken variational formulation and discretization

Let Ω_h be a mesh of the domain Ω, and $K \in \Omega_h$ denote any element in the mesh. As a standard technique in DPG methods [10], we consider broken test spaces, defined as

$$H^1(\Omega_h) = \{w \in L^2(\Omega) : w|_K \in H^1(K),\ K \in \Omega_h\}.$$

Similarly, we define $\boldsymbol{H}^1(\Omega_h) = [H^1(\Omega_h)]^2$. Then we consider test function $\boldsymbol{v} = \begin{pmatrix} v_1 \\ v_2 \end{pmatrix} \in \boldsymbol{H}^1(\Omega_h)$. Integrating by parts in each element and introducing interface traces as additional unknowns, we obtain the broken version of the ultraweak formulation:

$$\begin{cases} \boldsymbol{u} \in \boldsymbol{L}^2(\Omega), \hat{u}_n \in \mathrm{tr}_{\mathrm{div}} H(\mathrm{div}, \Omega), \hat{u}_t \in \mathrm{tr}_{\mathrm{curl}} H(\mathrm{curl}, \Omega) : \\ \qquad\qquad \hat{u}_n = \mu \qquad\quad \text{on } \Gamma, \\ -(\boldsymbol{u}, \nabla v_1) + \langle \hat{u}_n, v_1 \rangle_{\Gamma_h} = (f, v_1) \quad \forall v_1 \in H^1(\Omega_h), \\ (\boldsymbol{u}, \nabla \times v_2) + \langle \hat{u}_t, v_2 \rangle_{\Gamma_h} = (g, v_2) \quad \forall v_2 \in H^1(\Omega_h). \end{cases} \tag{10}$$

A few comments are in order. As detailed in [10], $\mathrm{tr}_{\mathrm{div}} H(\mathrm{div}, \Omega)$ is the normal trace of $H(\mathrm{div}, \Omega)$ onto the skeleton Γ_h of mesh Ω_h, while $\mathrm{tr}_{\mathrm{curl}} H(\mathrm{curl}, \Omega)$ is the tangential trace of $H(\mathrm{curl}, \Omega)$. Terms:

$$\langle \hat{u}_n, v_1 \rangle_{\Gamma_h} := \sum_{K \in \Omega_h} \langle \hat{u}_n, v_{1K} \rangle_{\partial K}, \qquad \langle \hat{u}_t, v_2 \rangle_{\Gamma_h} := \sum_{K \in \Omega_h} \langle \hat{u}_t, v_{2K} \rangle_{\partial K}$$

are the duality pairings on the mesh skeleton. The test norm is defined naturally by a sum:

$$\|\boldsymbol{v}\|^2_{\boldsymbol{H}^1(\Omega_h)} = \sum_{K \in \Omega_h} \|\boldsymbol{v}_K\|^2_{\boldsymbol{H}^1(K)}. \tag{11}$$

The well-posedness of the broken variational formulation (10) follows from its unbroken counterpart (8).

Finally, we discretize $\boldsymbol{L}^2(\Omega)$, the trace spaces, and test space $\boldsymbol{H}^1(\Omega_h)$ with exact sequence elements [22]. In particular, since DPG method can be viewed as a weighted least squares method for an *overdetermined* system, we use *enriched* test spaces: if we adopt piecewise polynomials of degree p for trial spaces[1], then we discretize test spaces with piecewise polynomials of degree $p + \Delta p$. In the reported numerical experiments, $\Delta p = 1$.

3 The adjoint operator within a closed operator framework

The introduced ultraweak formulation make use of A^*, the L^2 adjoint operator of A. In this section, we analyze A^* in a closed operator framework, and prove several properties relevant to the Closed Range Theorem for closed operators. These properties will come in handy as we study the well-posedness of the mixed problem in Section 4.

[1] In the exact sequence logic. This amounts to order p for an H^1-conforming finite element and order $p-1$ for an L^2-conforming finite element. $H(\mathrm{curl})$ and $H(\mathrm{div})$ finite element spaces contain all polynomials of order $p-1$, and some polynomials of order p.

3.1 Closed operator framework

First note that we can replace the inhomogeneous boundary condition (1c) with a homogeneous one, by introducing a lift $\boldsymbol{u}_0$ satisfying $\boldsymbol{u}_0 \cdot \boldsymbol{n} = \mu$ on Γ. In particular, we can seek $\boldsymbol{u}_0 = \nabla\phi$, and solve the Laplace problem with Neumann boundary condition for ϕ:

$$\begin{aligned} \Delta\phi &= 0 \quad \text{in } \Omega, \\ \frac{\partial\phi}{\partial n} &= \mu \quad \text{on } \Gamma. \end{aligned} \tag{12}$$

It is well known that there exists a unique solution $\phi \in H^1_m(\Omega) := \{\varphi \in H^1(\Omega) : \int_\Omega \varphi = 0\}$ to (12), and $\|\nabla\phi\| \le C\|\mu\|_{H^{-1/2}(\Gamma)}$ where C depends on the domain alone. Let $\boldsymbol{u} = \boldsymbol{u}_0 + \boldsymbol{w}$. Then $\boldsymbol{w}$ solves the div-curl system (1) with homogeneous boundary condition. Now define $A : \boldsymbol{L}^2(\Omega) \supset D(A) \to \boldsymbol{L}^2(\Omega)$ by

$$A\boldsymbol{u} := \begin{pmatrix} \operatorname{div}\boldsymbol{u} \\ \operatorname{curl}\boldsymbol{u} \end{pmatrix}, \tag{13}$$

with the domain $D(A) := H_0(\operatorname{div},\Omega) \cap H(\operatorname{curl},\Omega)$, where $H_0(\operatorname{div},\Omega)$ stands for $H(\operatorname{div},\Omega)$ functions with vanishing normal trace on Γ. As learned above, integration by parts allows us to find the *formal* L^2 adjoint of A, denoted by A^* and given by $A^*\boldsymbol{v} = -\nabla v_1 + \nabla \times v_2$. It can be verified that A is a closed operator, and $D(A)$ is dense in $\boldsymbol{L}^2(\Omega)$. Hence we can define the *real* adjoint operator of A, denoted by the same symbol, $A^* : \boldsymbol{L}^2(\Omega) \supset D(A^*) \to \boldsymbol{L}^2(\Omega)$, by the relation

$$(A\boldsymbol{u}, \boldsymbol{v}) = (\boldsymbol{u}, A^*\boldsymbol{v}) \quad \forall \boldsymbol{u} \in D(A), \tag{14}$$

and $D(A^*)$ is the maximal set for which (14) holds, i.e.,

$$D(A^*) = \{\boldsymbol{v} \in \boldsymbol{L}^2(\Omega) : A^*\boldsymbol{v} \in \boldsymbol{L}^2(\Omega), (A\boldsymbol{u}, \boldsymbol{v}) = (\boldsymbol{u}, A^*\boldsymbol{v}) \quad \forall \boldsymbol{u} \in D(A)\}. \tag{15}$$

The following proposition characterizes $D(A^*)$.

Proposition 1. *Suppose Ω has a piecewise $C^{1,1}$ boundary. Then $D(A^*) = H^1(\Omega) \times H^1_0(\Omega)$.*

To prove Proposition 1, we will need the lemma on orthogonal decomposition of $\boldsymbol{L}^2$ vector fields.

Lemma 1. *Suppose Ω satisfies the condition above. Then the following orthogonal decomposition holds:*

$$\boldsymbol{L}^2(\Omega) = G(\Omega) \oplus C_0(\Omega) \oplus \mathcal{H}_{n0}(\Omega)$$

where $G(\Omega) := \{\nabla\phi : \phi \in H^1(\Omega)\}$, $C_0(\Omega) := \{\nabla \times \psi : \psi \in H^1_0(\Omega)\}$, and $\mathcal{H}_{n0}(\Omega)$ represents normal harmonic vector fields, $\mathcal{H}_{n0}(\Omega) = \{\boldsymbol{u} \in \boldsymbol{L}^2(\Omega) : \operatorname{div}\boldsymbol{u} = 0, \operatorname{curl}\boldsymbol{u} = 0$ in $\Omega, \boldsymbol{u}\cdot\boldsymbol{n} = 0$ on $\Gamma\}$.

The proof of this lemma can be found as Theorem 3 in [3].

Proof of Proposition 1. First assume that $\boldsymbol{v} \in H^1(\Omega) \times H^1_0(\Omega)$. By Green's formula, we have for any $\boldsymbol{u} \in D(A)$,

$$\begin{aligned} (\operatorname{div}\boldsymbol{u}, v_1) + (\operatorname{curl}\boldsymbol{u}, v_2) &= (\boldsymbol{u}, -\nabla v_1) + \langle u_n, v_1\rangle_\Gamma + (\boldsymbol{u}, \nabla \times v_2) + \langle u_t, v_2\rangle_\Gamma \\ &= (\boldsymbol{u}, -\nabla v_1 + \nabla \times v_2) \end{aligned}$$

where the last equality follows from the fact that $u_n = 0$ and $v_2 = 0$ on Γ. Therefore $\boldsymbol{v} \in D(A^*)$, i.e., $D(A^*) \supset H^1(\Omega) \times H_0^1(\Omega)$.

To prove inclusion in the opposite direction, assume that $\boldsymbol{v} \in D(A^*)$, and let $\boldsymbol{g} := A^*\boldsymbol{v} = -\nabla v_1 + \nabla \times v_2 \in \boldsymbol{L}^2(\Omega)$. We first verify that $\boldsymbol{g} \perp \mathcal{H}_{n0}(\Omega)$ by direct computation: if $\boldsymbol{\eta} \in \mathcal{H}_{n0}(\Omega) \subset D(A)$, then $(\boldsymbol{\eta}, \boldsymbol{g}) = (\operatorname{div} \boldsymbol{\eta}, v_1) + (\operatorname{curl} \boldsymbol{\eta}, v_2) = 0$. Then Lemma 1 allows us to find $\phi \in H^1(\Omega), \psi \in H_0^1(\Omega)$ such that $\boldsymbol{g} = -\nabla\phi + \nabla \times \psi$. From the first part of the proof, we know that $\tilde{\boldsymbol{v}} = \begin{pmatrix} \phi \\ \psi \end{pmatrix} \in D(A^*)$ as well. Then $A^*(\tilde{\boldsymbol{v}} - \boldsymbol{v}) = 0$, i.e., $\tilde{\boldsymbol{v}} - \boldsymbol{v} \in \mathcal{N}(A^*)$.

Now we examine the null space of A^*. For $\boldsymbol{w} \in \mathcal{N}(A^*)$,

$$(\operatorname{div} \boldsymbol{u}, w_1) + (\operatorname{curl} \boldsymbol{u}, w_2) = 0 \quad \forall \boldsymbol{u} \in D(A). \tag{16}$$

In particular, we can select $\boldsymbol{u} \in D(A)$ to solve

$$\begin{aligned} \operatorname{div} \boldsymbol{u} &= w_1 - \overline{w_1}, \\ \operatorname{curl} \boldsymbol{u} &= w_2 \end{aligned} \tag{17}$$

where

$$\overline{w_1} = \frac{1}{m(\Omega)} \int_\Omega w_1$$

is the average of w_1. According to [3], such solution exists, and it is unique up to a harmonic vector field. Plugging (17) into (16), we get

$$(w_1 - \overline{w_1}, w_1) + (w_2, w_2) = 0.$$

Note that $w_1 - \overline{w_1}$ is L^2-orthogonal to any constant function, therefore $(w_1 - \overline{w_1}, w_1) = (w_1 - \overline{w_1}, w_1 - \overline{w_1})$, and

$$(w_1 - \overline{w_1}, w_1 - \overline{w_1}) + (w_2, w_2) = 0.$$

This implies that $w_1 = \overline{w_1}$, and hence is constant, and $w_2 = 0$. Thus

$$\mathcal{N}(A^*) = \{\boldsymbol{v} \in D(A^*) : v_1 = c, v_2 = 0, c \in \mathbb{R}\}. \tag{18}$$

With the characterization of $\mathcal{N}(A^*)$, we are finally ready to finish the proof. $\tilde{\boldsymbol{v}} - \boldsymbol{v} \in \mathcal{N}(A^*)$ implies that $v_1 = \phi + c$ and $v_2 = \psi$. Consequently, $v_1 \in H^1(\Omega)$ and $v_2 \in H_0^1(\Omega)$. □

3.2 Closed Range Theorem at work

We apply the Closed Range Theorem for closed operators [32] to the planar div-curl system. A is a densely defined closed operator, and A is bounded below in the quotient space [2, 3]:

$$\|A\boldsymbol{u}\| \geq \alpha \inf_{\boldsymbol{\eta} \in \mathcal{N}(A)} \|\boldsymbol{u} + \boldsymbol{\eta}\| \quad \forall \boldsymbol{u} \in D(A) \tag{19}$$

where $\mathcal{N}(A) = \mathcal{H}_{n0}(\Omega)$ has dimension J equal to the number of holes in the domain. Then $\mathcal{R}(A)$ is closed in $\boldsymbol{L}^2(\Omega)$, and $\mathcal{R}(A) = \mathcal{N}(A^*)^\perp$, where $\mathcal{N}(A^*)^\perp$ denotes the $\boldsymbol{L}^2$ orthogonal complement of $\mathcal{N}(A^*)$. Moreover, Closed Range Theorem tells us that $\mathcal{R}(A^*)$ is closed in $\boldsymbol{L}^2(\Omega)$, $\mathcal{R}(A^*) = \mathcal{N}(A)^\perp$, and A^* is bounded below with the same constant as A in the quotient space:

$$\|A^*\boldsymbol{v}\| \geq \alpha \inf_{\boldsymbol{\zeta} \in \mathcal{N}(A^*)} \|\boldsymbol{v} + \boldsymbol{\zeta}\| \quad \forall \boldsymbol{v} \in D(A^*). \tag{20}$$

The boundedness-below of A^* can also be analyzed directly.

4 Imposition of the circulation constraint

4.1 Least squares with linear constraints

The unconstrained residual minimization problem (3) is well posed if B is bounded below. However, for the div-curl problem in multiply connected domains, B admits a nontrivial kernel, and thus is not bounded below. We consider the constrained minimization problem instead:

$$\begin{aligned} \min_{\boldsymbol{u}\in\mathcal{U}} \quad & \frac{1}{2}\|B\boldsymbol{u}-l\|_{\mathcal{V}'}^2, \\ \text{s.t.} \quad & C\boldsymbol{u}=g. \end{aligned} \tag{21}$$

For the ultraweak formulation of div-curl problem, (8), we have $\mathcal{U}=\boldsymbol{L}^2(\Omega), \mathcal{V}=H^1(\Omega)\times H_0^1(\Omega)$, and $B:\mathcal{U}\to\mathcal{V}$ is given by

$$\langle B\boldsymbol{u},\boldsymbol{v}\rangle := b(\boldsymbol{u},\boldsymbol{v}) = (\boldsymbol{u},A^*\boldsymbol{v}) = (\boldsymbol{u},-\nabla v_1+\nabla\times v_2).$$

$C:\mathcal{U}\to\mathcal{Q}'$ represents a continuous linear constraint, where $\mathcal{Q}$ denotes some Hilbert space. In many cases, $\mathcal{Q}$ is finite dimensional. Equivalently, for a continuous bilinear form $c:\mathcal{U}\times\mathcal{Q}\to\mathbb{R}$, the constraint may be written in a variational form:

$$c(\boldsymbol{u},\boldsymbol{q}) = \langle C\boldsymbol{u},\boldsymbol{q}\rangle = g(\boldsymbol{q}) \quad \forall \boldsymbol{q}\in\mathcal{Q}. \tag{22}$$

Before discretization, when $l\in\mathcal{R}(B)$, the cost functional achieves a mimimum of 0 at any solution to $B\boldsymbol{u}=l$. Suppose we discretize trial space $\mathcal{U}$ with $\mathcal{U}_h\subset\mathcal{U}$. With *ideal* DPG, our approximate solution $\boldsymbol{u}_h^{\text{opt}}\in\mathcal{U}_h$ is defined to solve the constrained minimization problem:

$$\begin{aligned} \min_{\boldsymbol{u}_h\in\mathcal{U}_h} \quad & \frac{1}{2}\|B\boldsymbol{u}_h-l\|_{\mathcal{V}'}^2, \\ \text{s.t.} \quad & C\boldsymbol{u}_h=g. \end{aligned} \tag{23}$$

If B is bounded below, and the constraint set is assumed to satisfy certain conditions, the problem (23) admits a unique minimizer; see Appendix A in [26]. However, for the div-curl problem in multiply-connected domains, B has a nontrivial kernel, hence is not bounded below. The uniqueness of the minimizer is restored by introducing the constraint C. According to [3], the solution to the div-curl problem is unique up to a harmonic vector field. Thus it suffices to prescribe the $\boldsymbol{L}^2$ projection of $\boldsymbol{u}$ onto the space of harmonic vector fields, $\mathcal{H}_{n0}(\Omega)$. We can take $\mathcal{Q}=\mathcal{H}_{n0}(\Omega)\subset\boldsymbol{L}^2(\Omega)$, and define the constraint as

$$c(\boldsymbol{w},\boldsymbol{q}) := \int_\Omega \boldsymbol{w}\cdot\boldsymbol{q}, \tag{24}$$

Remark. $\dim\mathcal{H}_{n0}(\Omega)=J$, where J is the Betti number of the domain [3].

To deal with the dual norm in the cost function, we introduce the Riesz operator $R_{\mathcal{V}}:\mathcal{V}\to\mathcal{V}'$, and note that

$$\begin{aligned} \frac{1}{2}\|B\boldsymbol{u}-l\|_{\mathcal{V}'}^2 &= \frac{1}{2}\|R_{\mathcal{V}}^{-1}(B\boldsymbol{u}-l)\|_{\mathcal{V}}^2 = \frac{1}{2}(R_{\mathcal{V}}^{-1}B\boldsymbol{u},R_{\mathcal{V}}^{-1}B\boldsymbol{u})_{\mathcal{V}} - (R_{\mathcal{V}}^{-1}B\boldsymbol{u},R_{\mathcal{V}}^{-1}l)_{\mathcal{V}} + \frac{1}{2}\|R_{\mathcal{V}}^{-1}l\|_{\mathcal{V}}^2 \\ &= \frac{1}{2}\langle B\boldsymbol{u},R_{\mathcal{V}}^{-1}B\boldsymbol{u}\rangle_{\mathcal{V}',\mathcal{V}} - l(R_{\mathcal{V}}^{-1}B\boldsymbol{u}) + \frac{1}{2}\|l\|_{\mathcal{V}'}^2 = \frac{1}{2}b(\boldsymbol{u},R_{\mathcal{V}}^{-1}B\boldsymbol{u}) - B'R_{\mathcal{V}}^{-1}l(\boldsymbol{u}) + \frac{1}{2}\|l\|_{\mathcal{V}'}^2 \end{aligned} \tag{25}$$

Introduce the trial-to-test operator $T=R_{\mathcal{V}}^{-1}B:\mathcal{U}\to\mathcal{V}$, and a symmetric bilinear form on $\mathcal{U}$,

$$a(\boldsymbol{u},\boldsymbol{w}) := b(\boldsymbol{u},T\boldsymbol{w}) = (T\boldsymbol{u},T\boldsymbol{w})_{\mathcal{V}}. \tag{26}$$

Then

$$\frac{1}{2}\|B\boldsymbol{u}-l\|_{\mathcal{V}'}^2=\frac{1}{2}a(\boldsymbol{u},\boldsymbol{u})-f(\boldsymbol{u})+\frac{1}{2}\|l\|_{\mathcal{V}'}^2 \tag{27}$$

where $f=T'l=B'R_{\mathcal{V}}^{-1}l$.

Minimization of the residual (27) subject to the linear constraint (22) produces the following mixed system:

$$\begin{cases}\text{Find } \boldsymbol{u}\in\mathcal{U},\boldsymbol{p}\in\mathcal{Q}:\\ a(\boldsymbol{u},\boldsymbol{w})+c(\boldsymbol{w},\boldsymbol{p})=f(\boldsymbol{w}) & \forall\boldsymbol{w}\in\mathcal{U},\\ c(\boldsymbol{u},\boldsymbol{q})=g(\boldsymbol{q}) & \forall\boldsymbol{q}\in\mathcal{Q}.\end{cases} \tag{28}$$

Remark. With some abuse of symbols, the right hand sides f,g in (28) are not the same as the source term in div-curl system (1). However, this should not cause confusion since the right hand sides f,g in (28) will not be needed in later analysis.

Proposition 2. *The continuous mixed problem (28) for the div-curl system is well posed.*

Proof. We follow the classical Brezzi's theory [8] to establish the well-posedness of the mixed problem.

(LBB condition.)

$$\sup_{\boldsymbol{w}\in\mathcal{U}}\frac{|c(\boldsymbol{w},\boldsymbol{q})|}{\|\boldsymbol{w}\|}\geq\beta\|\boldsymbol{q}\| \tag{29}$$

is satisfied with $\beta=1$. Simply take $\boldsymbol{w}=\boldsymbol{q}$ and we achieve the supremum.

(Inf-sup in kernel condition.) First we characterize the kernel

$$\mathcal{U}_0=\{\boldsymbol{w}\in\mathcal{U}:c(\boldsymbol{w},\boldsymbol{q})=0,\forall\boldsymbol{q}\in\mathcal{Q}\}=\mathcal{H}_{n0}(\Omega)^{\perp}=\mathcal{N}(A)^{\perp}.$$

For $\boldsymbol{u}\in\mathcal{U}_0$, we have

$$\begin{aligned}\sup_{\boldsymbol{w}\in\mathcal{U}_0}\frac{|a(\boldsymbol{u},\boldsymbol{w})|}{\|\boldsymbol{w}\|}&\geq\frac{|a(\boldsymbol{u},\boldsymbol{u})|}{\|\boldsymbol{u}\|} && \text{(test with } \boldsymbol{u})\\ &=\frac{|b(\boldsymbol{u},T\boldsymbol{u})|}{\|\boldsymbol{u}\|} && \text{(definition of } a)\\ &=\frac{|b(\boldsymbol{u},T\boldsymbol{u})|}{\|T\boldsymbol{u}\|_{\mathcal{V}}}\frac{\|T\boldsymbol{u}\|_{\mathcal{V}}}{\|\boldsymbol{u}\|} && \text{(divide and multiply by } \|Tu\|_{\mathcal{V}})\\ &=\left(\sup_{\boldsymbol{v}\in\mathcal{V}}\frac{|b(\boldsymbol{u},\boldsymbol{v})|}{\|\boldsymbol{v}\|_{\mathcal{V}}}\right)\frac{\|T\boldsymbol{u}\|_{\mathcal{V}}}{\|\boldsymbol{u}\|} && (Tu \text{ achieves the best inf-sup constant})\\ &\geq\gamma^2\|\boldsymbol{u}\| && (B \text{ is bounded below on } \mathcal{U}_0)\end{aligned}$$

In the last step, we claim that B is bounded below on $\mathcal{U}_0$, i.e.,

$$\sup_{\boldsymbol{v}\in\mathcal{V}}\frac{|b(\boldsymbol{u},\boldsymbol{v})|}{\|\boldsymbol{v}\|_{\mathcal{V}}}=\sup_{\boldsymbol{v}\in\mathcal{V}}\frac{|(\boldsymbol{u},A^*\boldsymbol{v})|}{\|\boldsymbol{v}\|_{\mathcal{V}}}\geq\gamma\|\boldsymbol{u}\|\quad\forall\boldsymbol{u}\in\mathcal{H}_{n0}(\Omega)^{\perp}. \tag{30}$$

To prove (30), we choose $\boldsymbol{v}=\boldsymbol{z}$ to solve the adjoint problem $A^*\boldsymbol{z}=\boldsymbol{u}$. This problem is solvable because $\boldsymbol{u}\in\mathcal{H}_{n0}(\Omega)^{\perp}=\mathcal{N}(A)^{\perp}=\mathcal{R}(A^*)$, and by Closed Range Theorem

$$\|\boldsymbol{u}\|=\|A^*\boldsymbol{z}\|\geq\alpha\|\boldsymbol{z}\| \tag{31}$$

for the particular $\boldsymbol{z}$ with minimum L^2 norm. Therefore,

$$\|\boldsymbol{z}\|_{\mathcal{V}}^2=\|\boldsymbol{z}\|^2+\|A^*\boldsymbol{z}\|^2\leq(\alpha^{-2}+1)\|\boldsymbol{u}\|^2, \tag{32}$$

and

$$\sup_{\boldsymbol{v}\in\mathcal{V}} \frac{|(\boldsymbol{u}, A^*\boldsymbol{v})|}{\|\boldsymbol{v}\|_{\mathcal{V}}} \geq \frac{(\boldsymbol{u}, A^*\boldsymbol{z})}{\|\boldsymbol{z}\|_{\mathcal{V}}} \geq (\alpha^{-2}+1)^{-\frac{1}{2}}\|\boldsymbol{u}\|. \tag{33}$$

Thus (30) holds with $\gamma = (\alpha^{-2}+1)^{-\frac{1}{2}}$.

(Compatibility condition.)

$$\mathcal{U}_{00} := \{\boldsymbol{w}_0 \in \mathcal{U}_0 : a(\boldsymbol{u}_0, \boldsymbol{w}_0) = 0 \quad \forall \boldsymbol{u}_0 \in \mathcal{U}_0\}. \tag{34}$$

Note that $a(\boldsymbol{u}_0, \boldsymbol{w}_0) = (T\boldsymbol{u}_0, T\boldsymbol{w}_0) = 0$. Testing with $\boldsymbol{u}_0 = \boldsymbol{w}_0$, we get $T\boldsymbol{w}_0 = 0$, or equivalently, $B\boldsymbol{w}_0 = 0$ since $R_{\mathcal{V}}^{-1}$ is an isomorphism. This implies

$$b(\boldsymbol{w}_0, \boldsymbol{v}) = (\boldsymbol{w}_0, A^*\boldsymbol{v}) = 0 \quad \forall \boldsymbol{v} \in D(A^*).$$

Therefore, $(A\boldsymbol{w}_0, \boldsymbol{v}) = (\boldsymbol{w}_0, A^*\boldsymbol{v}) = 0$, i.e., $\boldsymbol{w}_0 \in \mathcal{N}(A)$. Recall that $\mathcal{U}_0 = \mathcal{N}(A)^\perp$. Then $\boldsymbol{w}_0 \in \mathcal{N}(A)^\perp \cap \mathcal{N}(A) = \{0\}$. The compatibility condition is always satisfied. □

4.2 Circulation constraint

The constraint (24) requires the knowledge of $\mathcal{Q} = \mathcal{H}_{n0}(\Omega)$. However, in general, we do not have an analytical expression for the harmonic vector fields $\mathcal{H}_{n0}(\Omega)$. So in actual computation, we choose to work with an equivalent formulation of the constraint, i.e., prescription of the circulation around Γ_1 [3]. For the sake of completeness, we recall some key results from [3].

Consider a general multiply-connected domain Ω, whose boundary is piecewise $C^{1,1}$ and Betti number is J. The outer boundary is denoted by Γ_0 and inner boundaries are $\Gamma_1, \cdots, \Gamma_J$. Then $\dim \mathcal{H}_{n0}(\Omega) = J$, and let $\{\boldsymbol{k}^{(1)}, \cdots, \boldsymbol{k}^{(J)}\}$ denote the particular basis of $\mathcal{H}_{n0}(\Omega)$ defined by (52) in [3]. When $J \geq 1$ and $\boldsymbol{w} \in \boldsymbol{L}^2(\Omega)$, the projection of $\boldsymbol{w}$ onto $\mathcal{H}_{n0}(\Omega)$ is given by

$$P\boldsymbol{w} = \sum_{j=1}^{J} c_j \boldsymbol{k}^{(j)} \tag{35}$$

where $(c_1, \cdots, c_J)$ is the solution of linear system

$$(P\boldsymbol{w}, \boldsymbol{k}^{(l)}) = \sum_{j=1}^{J} k_{lj} c_j = (\boldsymbol{w}, \boldsymbol{k}^{(l)}), \quad 1 \leq l \leq J. \tag{36}$$

Here $k_{lj} = (\boldsymbol{k}^{(l)}, \boldsymbol{k}^{(j)})$ is the component of a Gram matrix. We invoke (64) in [3] as the following lemma.

Lemma 2. *For $1 \leq j, l \leq J$,*

$$\int_{\Gamma_j} \boldsymbol{k}^{(l)} \cdot \boldsymbol{t} = \int_{\Gamma_l} \boldsymbol{k}^{(j)} \cdot \boldsymbol{t} = -(\boldsymbol{k}^{(j)}, \boldsymbol{k}^{(l)}).$$

If $\boldsymbol{w}$ is irrotational, as in the case of flow around airfoil problem, then

$$\int_{\Gamma_l} \boldsymbol{w} \cdot \boldsymbol{t} = \int_{\Gamma_l} P\boldsymbol{w} \cdot \boldsymbol{t} = \sum_{j=1}^{J} c_j \int_{\Gamma_l} \boldsymbol{k}^{(j)} \cdot \boldsymbol{t} = -\sum_{j=1}^{J} k_{lj} c_j. \tag{37}$$

See (70) in [3] for a proof. Plugging (36) into (37), we get

$$\int_{\Gamma_l} \boldsymbol{w} \cdot \boldsymbol{t} = -(\boldsymbol{w}, \boldsymbol{k}^{(l)}), \quad 1 \leq l \leq J \tag{38}$$

when $\boldsymbol{w}$ is irrotational. Therefore, prescription of the circulation around $\Gamma_1, \cdots, \Gamma_J$ is equivalent to specifying the projection of $\boldsymbol{w}$ onto $\mathcal{H}_{n0}(\Omega)$. When $\boldsymbol{w}$ is not curl free, as the case in some numerical experiments, prescribing the circulation still fixes the projection onto $\mathcal{H}_{n0}(\Omega)$. The only difference is that (38) now becomes

$$\int_{\Gamma_l} \boldsymbol{w} \cdot \boldsymbol{t} = -(\boldsymbol{w}, \boldsymbol{k}^{(l)}) + \int_{\Gamma_l} (\nabla \times \psi) \cdot \boldsymbol{t} \tag{39}$$

where $\psi \in H_0^1(\Omega)$, $\nabla \times \psi$ is the rotational part of $\boldsymbol{w}$, which is determined uniquely from $\operatorname{curl} \boldsymbol{w}$.

In the case of a doubly-connected domain, $J = 1$ and we have only one circulation to prescribe. From now on, we focus on doubly-connected domains for ease of presentation, although the framework is general. Note that, however, in the ultraweak formulation (8), $\boldsymbol{u}$ is only assumed to be $\boldsymbol{L}^2(\Omega)$, we cannot talk about its tangential trace, let alone circulation. We must test with functions outside of $D(A^*) = H^1(\Omega) \times H_0^1(\Omega)$, and introduce $\hat{u}_t$, the tangential trace of $H(\operatorname{curl}, \Omega)$ functions onto Γ_1 (denoted by $\operatorname{tr}_{t,\Gamma_1} H(\operatorname{curl}, \Omega)$), as an additional unknown.

Ultraweak formulation with tangential trace unknown.

$$\begin{cases} \boldsymbol{u} \in \boldsymbol{L}^2(\Omega), \hat{u}_t \in \operatorname{tr}_{t,\Gamma_1} H(\operatorname{curl}, \Omega) : & \\ \qquad\qquad -(\boldsymbol{u}, \nabla v_1) = (f, v_1) - \langle \mu, v_1 \rangle_\Gamma & \forall v_1 \in H^1(\Omega), \\ (\boldsymbol{u}, \nabla \times v_2) + \langle \hat{u}_t, v_2 \rangle_{\Gamma_1} = (g, v_2) & \forall v_2 \in H^1_{\Gamma_0}(\Omega) \end{cases} \tag{40}$$

where $H^1_{\Gamma_0}(\Omega) := \{\varphi \in H^1(\Omega) : \varphi|_{\Gamma_0} = 0\}$. $\hat{u}_t \in \hat{\mathcal{U}} := \operatorname{tr}_{t,\Gamma_1} H(\operatorname{curl}, \Omega) = H^{-1/2}(\Gamma_1)$ is measured by the minimum energy extension norm [10], denoted as $\|\hat{u}_t\|_{\hat{\mathcal{U}}}$. The group solution variable $(\boldsymbol{u}, \hat{u}_t)$ can be measured in any product norm (as they are equivalent), e.g., $\|(\boldsymbol{u}, \hat{u}_t)\|_{\mathcal{U} \times \hat{\mathcal{U}}} := \|\boldsymbol{u}\| + \|\hat{u}_t\|_{\hat{\mathcal{U}}}$. We analyze the problem (40) with the circulation constraint as:

$$\int_{\Gamma_1} \hat{u}_t = \kappa \tag{41}$$

where the integral is understood in the sense of duality pairing:

$$\int_{\Gamma_1} \hat{u}_t := \langle \hat{u}_t, 1 \rangle_{\Gamma_1}.$$

We would like to reproduce the argument from Proposition 2, i.e., (40) understood in the sense of minimum residual with the constraint (41) is a well-posed mixed problem. In this case, $\mathcal{Q} = \mathbb{R}$ and the Lagrange multiplier is a scalar.

Proposition 3. *The constrained residual minimization problem (21), with B determined from (40) and constraint C as the circulation (41), is well posed.*

Proof. (LBB condition.) Let $\boldsymbol{w} \in H(\operatorname{curl}, \Omega)$ be the minimum energy extension of $\hat{w}_t = 1$ on Γ_1. Then $\|\hat{w}_t\|_{\hat{\mathcal{U}}} = \|\boldsymbol{w}\|_{H(\operatorname{curl},\Omega)} > 0$, and

$$\sup_{\hat{u}_t \in \hat{\mathcal{U}}} \frac{\langle \hat{u}_t, 1 \rangle_{\Gamma_1}}{\|\hat{u}_t\|_{\hat{\mathcal{U}}}} \geq \frac{\langle \hat{w}_t, 1 \rangle_{\Gamma_1}}{\|\hat{w}_t\|_{\hat{\mathcal{U}}}} = \frac{\operatorname{length}(\Gamma_1)}{\|\boldsymbol{w}\|_{H(\operatorname{curl},\Omega)}} > 0. \tag{42}$$

(Inf-sup in kernel condition.) We follow exactly the same argument as in the proof of Proposition 2. It remains to prove that the bilinear form satisfies the inf-sup condition:

$$\sup_{\boldsymbol{v} \in \mathcal{V}} \frac{(\boldsymbol{u}, A^* \boldsymbol{v}) + \langle \hat{u}_t, v_2 \rangle_{\Gamma_1}}{\|\boldsymbol{v}\|_{\mathcal{V}}} \geq \gamma'(\|\boldsymbol{u}\| + \|\hat{u}_t\|_{\hat{\mathcal{U}}}) \tag{43}$$

for all $\boldsymbol{u} \in \boldsymbol{L}^2(\Omega)$, $\hat{u}_t \in \hat{\mathcal{U}}$ satisfying $\langle \hat{u}_t, 1\rangle_{\Gamma_1} = 0$, with some constant $\gamma' > 0$. Here $\mathcal{V} := H^1(\Omega) \times H^1_{\Gamma_0}(\Omega)$ and is equipped with the same norm as before; see (9). We define a functional $l \in \mathcal{V}'$ by

$$l(\boldsymbol{v}) := (\boldsymbol{u}, A^*\boldsymbol{v}) + \langle \hat{u}_t, v_2\rangle_{\Gamma_1} \quad \forall \boldsymbol{v} \in \mathcal{V}. \tag{44}$$

Then it suffices to show that both $\|\boldsymbol{u}\|$ and $\|\hat{u}_t\|_{\hat{\mathcal{U}}}$ are bounded above by $\|l\|_{\mathcal{V}'}$. Let $\boldsymbol{u} = \boldsymbol{u}_{\mathcal{H}} + \boldsymbol{u}_{\mathcal{H}^\perp}$ be the orthogonal decomposition of the $\boldsymbol{L}^2$ vector field $\boldsymbol{u}$ into a harmonic vector field $\boldsymbol{u}_{\mathcal{H}} \in \mathcal{H}_{n0}(\Omega)$, and a part $\boldsymbol{u}_{\mathcal{H}^\perp} \in \mathcal{H}_{n0}(\Omega)^\perp$. From the Pythagorean Theorem, we have $\|\boldsymbol{u}\|^2 = \|\boldsymbol{u}_{\mathcal{H}}\|^2 + \|\boldsymbol{u}_{\mathcal{H}^\perp}\|^2$. Thus we only need to control $\|\boldsymbol{u}_{\mathcal{H}}\|$ and $\|\boldsymbol{u}_{\mathcal{H}^\perp}\|$ separately. Testing with $\boldsymbol{v} \in D(A^*)$ in (44), we get

$$l(\boldsymbol{v}) = (\boldsymbol{u}, A^*\boldsymbol{v}) = (\boldsymbol{u}_{\mathcal{H}}, A^*\boldsymbol{v}) + (\boldsymbol{u}_{\mathcal{H}^\perp}, A^*\boldsymbol{v}) \tag{45}$$

since $v_2 = 0$ on Γ for $\boldsymbol{v} \in D(A^*)$. Note that $\boldsymbol{u}_{\mathcal{H}} \in \mathcal{H}_{n0}(\Omega) = \mathcal{N}(A) \subset D(A)$; hence

$$(\boldsymbol{u}_{\mathcal{H}}, A^*\boldsymbol{v}) = (A\boldsymbol{u}_{\mathcal{H}}, \boldsymbol{v}) = 0 \quad \forall \boldsymbol{v} \in D(A^*). \tag{46}$$

Plugging (46) into (45), we get

$$l(\boldsymbol{v}) = (\boldsymbol{u}_{\mathcal{H}^\perp}, A^*\boldsymbol{v}) \quad \forall \boldsymbol{v} \in D(A^*). \tag{47}$$

From (30), we have

$$\|\boldsymbol{u}_{\mathcal{H}^\perp}\| \le \gamma^{-1} \sup_{\boldsymbol{v}\in D(A^*)} \frac{|(\boldsymbol{u}_{\mathcal{H}^\perp}, A^*\boldsymbol{v})|}{\|\boldsymbol{v}\|_{\mathcal{V}}} = \gamma^{-1} \sup_{\boldsymbol{v}\in \mathcal{V}} \frac{|l(\boldsymbol{v})|}{\|\boldsymbol{v}\|_{\mathcal{V}}} = \gamma^{-1}\|l\|_{\mathcal{V}'}. \tag{48}$$

Now we examine $\|\boldsymbol{u}_{\mathcal{H}}\|$. To that end, we recall that in a doubly-connected domain, $\dim \mathcal{H}_{n0}(\Omega) = 1$, and one basis $\{\boldsymbol{k}^{(1)}\}$ is given by $\boldsymbol{k}^{(1)} = \nabla \times \psi$, where $\psi \in H^1(\Omega)$ solves the Laplace problem with Dirichlet boundary condition [3]:

$$\begin{aligned} \Delta\psi &= 0 \quad \text{in } \Omega, \\ \psi &= 0 \quad \text{on } \Gamma_0, \\ \psi &= 1 \quad \text{on } \Gamma_1. \end{aligned} \tag{49}$$

Assume $\boldsymbol{u}_{\mathcal{H}} = \lambda \boldsymbol{k}^{(1)}$ for some $\lambda \in \mathbb{R}$. We test (44) with $v_1 = 0, v_2 = \psi$, note that $\langle \hat{u}_t, 1\rangle_{\Gamma_1} = 0$, and we obtain

$$l(\boldsymbol{v}) = (\boldsymbol{u}, A^*\boldsymbol{v}) = (\boldsymbol{u}, \nabla \times \psi) = (\boldsymbol{u}_{\mathcal{H}} + \boldsymbol{u}_{\mathcal{H}^\perp}, \nabla \times \psi) \tag{50}$$

where $\boldsymbol{v} = (0, \psi)$. The definition of $\boldsymbol{u}_{\mathcal{H}^\perp}$ guarantees that $(\boldsymbol{u}_{\mathcal{H}^\perp}, \nabla \times \psi) = (\boldsymbol{u}_{\mathcal{H}^\perp}, \boldsymbol{k}^{(1)}) = 0$. Thus

$$l(\boldsymbol{v}) = (\boldsymbol{u}_{\mathcal{H}}, \nabla \times \psi) = \lambda(\nabla \times \psi, \nabla \times \psi) = \|\boldsymbol{u}_{\mathcal{H}}\|\|\nabla \times \psi\|.$$

Dividing both sides by $\|\nabla \times \psi\|$, we get

$$\|\boldsymbol{u}_{\mathcal{H}}\| = \frac{l(\boldsymbol{v})}{\|\nabla \times \psi\|} = \alpha \frac{l(\boldsymbol{v})}{\|\boldsymbol{v}\|_{\mathcal{V}}} \le \alpha \|l\|_{\mathcal{V}'} \tag{51}$$

where

$$\alpha = \frac{\|\boldsymbol{v}\|_{\mathcal{V}}}{\|\nabla \times \psi\|} = \frac{(\|\psi\|^2 + \|\nabla \times \psi\|^2)^{1/2}}{\|\nabla \times \psi\|} > 1$$

is a constant.

Having controlled both $\|\boldsymbol{u}_{\mathcal{H}}\|$ and $\|\boldsymbol{u}_{\mathcal{H}^\perp}\|$, in (51) and (48) respectively, we are now in a position to bound $\|\hat{u}_t\|_{\hat{\mathcal{U}}}$. Here we use the "Brezzi's trick".

$$\|\hat{u}_t\|_{\hat{\mathcal{U}}} := \sup_{v_2 \in H^1_{\Gamma_0}(\Omega)} \frac{|\langle \hat{u}_t, v_2 \rangle_{\Gamma_1}|}{\|v_2\|_{H^1(\Omega)}} = \sup_{\boldsymbol{v} \in \mathcal{V}} \frac{|l(\boldsymbol{v}) - (\boldsymbol{u}, A^*\boldsymbol{v})|}{\|\boldsymbol{v}\|_{\mathcal{V}}} \leq \|l\|_{\mathcal{V}'} + \|\boldsymbol{u}\| \frac{\|A^*\boldsymbol{v}\|}{\|\boldsymbol{v}\|_{\mathcal{V}}} \leq (1 + (\gamma^{-2} + \alpha^2)^{1/2}) \|l\|_{\mathcal{V}'} \quad (52)$$

where in the last inequality we have used the fact that $\frac{\|A^*\boldsymbol{v}\|}{\|\boldsymbol{v}\|_{\mathcal{V}}} \leq 1$ and $\|\boldsymbol{u}\| = (\|\boldsymbol{u}_{\mathcal{H}^\perp}\|^2 + \|\boldsymbol{u}_{\mathcal{H}}\|^2)^{1/2}$.

(Compatibility condition.) Similar to the argument for the inf-sup in kernel condition, we decompose $\boldsymbol{w}_0$ into $\boldsymbol{w}_{0\mathcal{H}}$ and $\boldsymbol{w}_{0\mathcal{H}^\perp}$, and test

$$(\boldsymbol{w}_0, A^*\boldsymbol{v}) + \langle \hat{w}_{0t}, v_2 \rangle_{\Gamma_1} = 0$$

with $\boldsymbol{v} \in D(A^*)$ and $v_1 = 0, v_2 = \nabla \times \psi$ respectively, to conclude that both $\boldsymbol{w}_{0\mathcal{H}}$ and $\boldsymbol{w}_{0\mathcal{H}^\perp}$ are 0. Finally test with general $\boldsymbol{v} \in \mathcal{V}$ to conclude that the tangential trace $\hat{w}_{0t} = 0$. Thus $\mathcal{U}_{00}$ is trivial; compatibility condition is automatically satisfied. □

Remark. The analysis of the mixed problem for the broken ultraweak formulation (10) with circulation constraint (41) is analogous. We refer readers to [10] for detailed techniques to treat broken formulations.

4.3 Discrete stability

Ideal DPG seeks the minimizer of (23) in the discrete finite element space $\mathcal{U}_h$. This leads to the discrete mixed problem:

$$\begin{cases} \text{Find } \boldsymbol{u}_h \in \mathcal{U}_h, \boldsymbol{p} \in \mathcal{Q} : \\ a(\boldsymbol{u}_h, \boldsymbol{w}) + c(\boldsymbol{w}, \boldsymbol{p}) = f(\boldsymbol{w}) \quad \forall \boldsymbol{w} \in \mathcal{U}, \\ c(\boldsymbol{u}_h, \boldsymbol{q}) \qquad\qquad = g(\boldsymbol{q}) \quad \forall \boldsymbol{q} \in \mathcal{Q}. \end{cases} \quad (53)$$

The bilinear form a is determined from the broken ultraweak formulation (10), and constraint is (41). To establish the convergence of our solution, we have to show that the LBB condition and inf-sup in kernel condition are satisfied for some bounded-below constants uniformly.

Proposition 4. *The discrete mixed problem (53) for the div-curl system satisfies the discrete inf-sup conditions. Therefore, according to Brezzi's Theorem, the numerical solution $\boldsymbol{u}_h$ converges to $\boldsymbol{u}$ at the optimal rate determined by the interpolation error estimate.*

Proof. The discrete LBB condition is satisfied, which can be proved in a way similar to (42). The difference is that we now lift the trace $\hat{w}_t = 1$ on Γ_1 into a discrete subspace, $\boldsymbol{w}_h \in Q^h \subset H(\text{curl}, \Omega)$. As we refine the mesh, the space Q^h becomes bigger, and the minimum energy extension norm $\|\boldsymbol{w}_h\|_{H(\text{curl},\Omega)}$ decreases. The LBB constant only improves as the mesh gets refined.

The discrete inf-sup in kernel condition is not an issue, since ideal DPG only keeps or improves the continuous inf-sup constant [16]. □

Remark. The *practical* DPG method enjoys the same property described in Proposition 4 for ideal DPG, as we are employing standard exact sequence elements and Fortin operators can be constructed. See [23, 17].

5 Numerical results

5.1 Smooth solution in a unit square

As verification, we first compute the numerical solution of div-curl system in a unit square, $\Omega = [0,1]^2$. The manufactured solution $\boldsymbol{u} = \begin{pmatrix} u_1 \\ u_2 \end{pmatrix}$ is defined as

$$u_1 = -\pi \sin(\pi x_1) \exp(\pi x_2), \; u_2 = \pi \cos(\pi x_1) \exp(\pi x_2). \tag{54}$$

$\boldsymbol{u}$ is solenoidal and irrotational, and can be obtained by solving a Laplace problem. This amounts to setting $f = 0$, $g = 0$ in (1), and the normal trace $u_n = \mu$ is set according to the manufactured solution. No circulation constraint needs to be imposed, since the domain is simply-connected. We start with a mesh consisting of one quadrilateral element, and perform uniform h-refinements. Fig. 2 shows L^2 relative error versus degrees of freedom for different polynomial degrees. The observed convergence rates are perfectly aligned with theory:

$$\|\boldsymbol{u} - \boldsymbol{u}_h\| \leq C h^r |\boldsymbol{u}|_{\boldsymbol{H}^r(K)} \tag{55}$$

if $p \geq r$. As the solution is smooth, the convergence rate is determined only by the polynomial order.

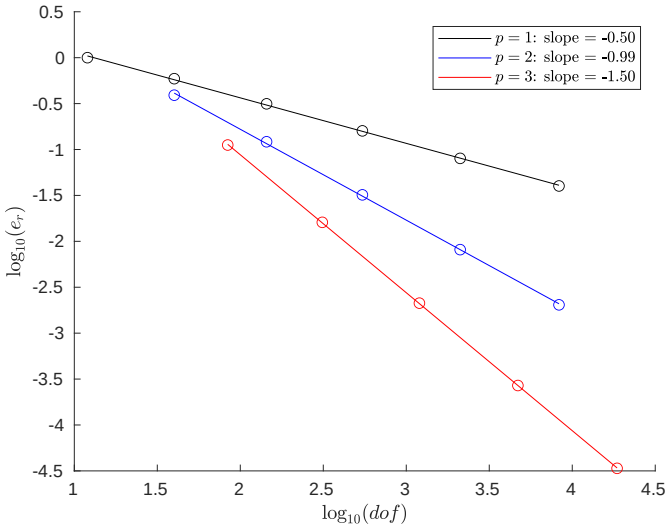

Figure 2: Relative error measured in $\boldsymbol{L}^2$ norm versus degrees of freedom. The black line corresponds to $p = 1$, blue for $p = 2$, and red for $p = 3$. Slopes are computed by linear regression.

Adaptivity. As detailed in [11], DPG comes with a built-in a posteriori error estimator, i.e., $\|\psi\|^2_{\mathcal{V}}$, which we utilize to perform adaptive refinements. After solving for $\mathfrak{u}_h$, we compute the error representation function for each element K during post-processing:

$$(\boldsymbol{\psi}_K, \boldsymbol{v}_K)_{\mathcal{V}(K)} = l(\boldsymbol{v}_K) - \mathfrak{b}(\mathfrak{u}_h, \boldsymbol{v}_K) \quad \forall \boldsymbol{v}_K \in \mathcal{V}_h(K)$$

where $\mathfrak{u}_h := (\boldsymbol{u}_h, \hat{\boldsymbol{u}}_h)$ denotes the group variable, $\mathfrak{b}(\mathfrak{u}_h, \boldsymbol{v}_K) := (\boldsymbol{u}_h, A^*\boldsymbol{v}_K)_{\boldsymbol{L}^2(K)} + \langle \hat{\boldsymbol{u}}_h, \boldsymbol{v}_K \rangle_{\partial K}$, see (10); $\mathcal{V}(K) = \boldsymbol{H}^1(K)$, and $\mathcal{V}_h(K)$ represents the polynomial space to discretize $\boldsymbol{H}^1(K)$. Here $\boldsymbol{\psi}_K = \begin{pmatrix} \psi_{1K} \\ \psi_{2K} \end{pmatrix}$ has two components. We compute $\|\boldsymbol{\psi}_K\|^2_{\mathcal{V}(K)}$ and use it as an a posteriori error estimator. For ideal DPG with unbroken ultraweak formulation,

$$\|\boldsymbol{\psi}\|^2_{\mathcal{V}} = \|l - B\boldsymbol{u}_h\|^2_{\mathcal{V}'} = \|B(\boldsymbol{u} - \boldsymbol{u}_h)\|^2_{\mathcal{V}'} = \|\boldsymbol{u} - \boldsymbol{u}_h\|^2_E$$

where the energy norm $\|\cdot\|_E$ is defined as

$$\|\boldsymbol{w}\|_E := \sup_{\boldsymbol{v}\in\mathcal{V}} \frac{|b(\boldsymbol{w}, \boldsymbol{v})|}{\|\boldsymbol{v}\|_{\mathcal{V}}} = \sup_{\boldsymbol{v}\in\mathcal{V}} \frac{|(\boldsymbol{w}, A^*\boldsymbol{v})|}{\|\boldsymbol{v}\|_{\mathcal{V}}}$$

and can be shown to be equivalent to the $\boldsymbol{L}^2$ norm; see (9) and (33). In actual computation, we use broken test spaces and practical DPG (discretize the test space), but we still observe very good agreement between the residual $\|\boldsymbol{\psi}\|_{\boldsymbol{H}^1(\Omega_h)}$ and the $\boldsymbol{L}^2$ error. We start with a single element of order $p = 2$, and perform h-adaptive refinements with a greedy strategy. Fig. 3(a) plots relative error and residual versus degrees of freedom, while Fig. 3(b) plots the contours of the numerical solution u_1 on the final mesh. To make clear the efficiency and reliability of our error indicator, in Table 1 we document the ratio of residual $\|\psi\|_{\mathcal{V}}$ to error $\|\boldsymbol{u} - \boldsymbol{u}_h\|$. The maximal discrepancy is only 7.3%.

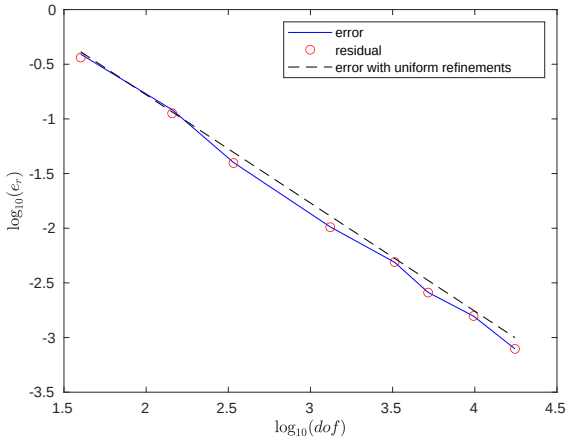

(a) Relative $\boldsymbol{L}^2$ error and residual versus degrees of freedom. The blue solid line represents relative error $\|\boldsymbol{u} - \boldsymbol{u}_h\|/\|\boldsymbol{u}\|$, red circles represent scaled residual $\|\boldsymbol{\psi}\|_{\mathcal{V}}/\|\boldsymbol{u}\|$, and the black dashed line stands for relative error with uniform refinements.

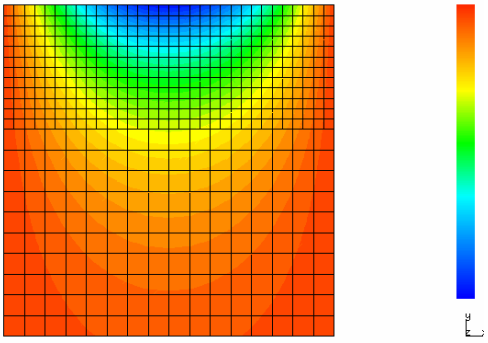

(b) Contour plot of u_1 on the final mesh.

Figure 3: Adaptive refinement study.

dof	40	144	340	1320	3252	5200	9824	17560
residual/error	0.9333	0.9268	0.9876	0.9933	1.0045	0.9965	1.0029	1.0000

Table 1: The ratio of residual to error along refinement.

5.2 Solenoidal and irrotational solution in a toroidal domain

Now we examine a solenoidal and irrotational solution in a toroidal domain, $\Omega = \left(-1, \frac{1}{2}\right)^2 \setminus \left[-\frac{1}{2}, 0\right]^2$. The exact solution is given in polar coordinates by

$$u_r = 0, \quad u_\theta = \frac{1}{2\pi r}$$

where the origin of the polar coordinates is at $(-\frac{1}{4}, -\frac{1}{4})$. The relation between Cartesian coordinates (x_1, x_2) and polor coordinates (r, θ) is given by

$$x_1 + \frac{1}{4} = r\cos\theta, \quad x_2 + \frac{1}{4} = r\sin\theta.$$

Note that the circulation of this manufactured solution is *nonzero*, and we impose the correct circulation as the constraint. We start with 8 square elements of order $p = 2$, and perform both uniform refinements and h-adaptive refinements with a greedy strategy. Fig. 4(a) plots relative error and residual versus degrees of freedom, and Fig. 4(b) plots the contours of the numerical solution u_1 on the final adaptive mesh. In Table 2 we record the ratio of residual to error along adaptive refinement. Similar to the previous case, the residual $\|\psi\|_{\mathcal{V}}$ is a very good error estimator even in *multiply-connected* domains: except for the first very coarse mesh, the discrepancy between residual and error is less than 2%.

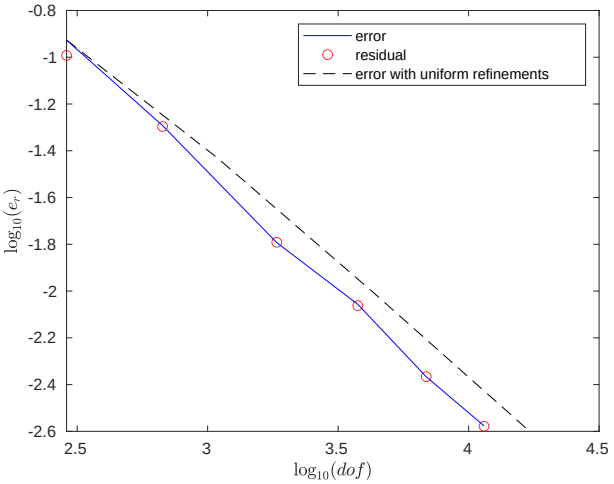

(a) Relative $\boldsymbol{L}^2$ error and residual versus degrees of freedom. The blue solid line represents relative error $\|\boldsymbol{u} - \boldsymbol{u}_h\|/\|\boldsymbol{u}\|$, red circles represent scaled residual $\|\boldsymbol{\psi}\|_{\mathcal{V}}/\|\boldsymbol{u}\|$, and the black dashed line stands for relative error with uniform refinements.

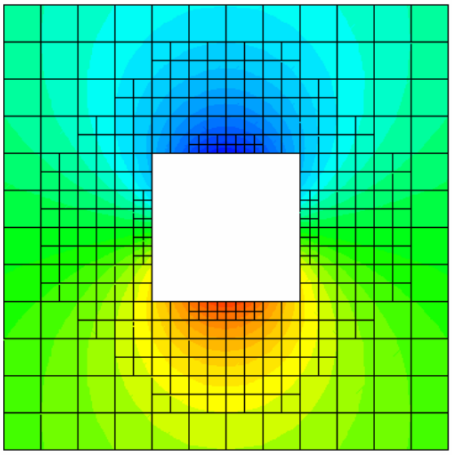

(b) Contour plot of u_1 on the final adaptive mesh.

Figure 4: Uniform and adaptive refinement study.

dof	288	672	1840	3760	6880	11456
residual/error	0.8598	0.9908	1.0025	0.9868	1.0005	0.9957

Table 2: The ratio of residual to error along adaptive refinement.

5.3 Solenoidal solution in a toroidal domain

Following [9] (Example 5 therein), we study smooth and singular solutions in a toroidal domain. $\Omega = \left(-1, \frac{1}{2}\right)^2 \setminus \left[-\frac{1}{2}, 0\right]^2$, and the manufactured solution is given by

$$\boldsymbol{u} = \nabla \times r^\gamma \sin(\alpha\theta) = \alpha r^{\gamma-1}\cos(\alpha\theta)\,\hat{\boldsymbol{e}}_r - \gamma r^{\gamma-1}\sin(\alpha\theta)\,\hat{\boldsymbol{e}}_\theta \tag{56}$$

where r, θ are polar coordinates with the same origin as the Cartesian coordinates, and $\alpha = 1, 2, 3, \cdots$, $\gamma > 0$. It can be verified that $\boldsymbol{u} \in \boldsymbol{H}^{\gamma-\epsilon}(\Omega)$ for $\gamma \neq 1$, and is singular at the origin if $\gamma < 1$. The curl of $\boldsymbol{u}$ can be computed as

$$\operatorname{curl} \boldsymbol{u} = -\Delta\big(r^\gamma \sin(\alpha\theta)\big) = (\alpha^2 - \gamma^2) r^{\gamma-2}\sin(\alpha\theta)$$

$\operatorname{curl} \boldsymbol{u} \notin L^2(\Omega)$ when $\gamma < 1$. We choose $\alpha = 2$ and experiment with three different values of γ: $\gamma = 1.25, 1, 2/3$. We start with a mesh consisting of 8 square elements with order $p = 3$ and perform uniform h-refinements. Fig. 5(a–c) illustrates the different convergence rates for solutions with different regularity. The convergence rates are $-1.25, -1, -0.66$, respectively, matching the regularity of the solution. In contrast with the asymptotic optimal rates observed in [9], our method achieves the optimal rate from day one, on a very coarse mesh. Fig. 5(d) displays one solution obtained for $\gamma = 2/3$ and $h = 1/8$.

5.4 A solution that is neither solenoidal nor irrotational

On the same mesh as in Section 5.3, we consider the manufactured solution

$$\boldsymbol{u} = \nabla \times r^\gamma \sin(\alpha\theta) + \beta \begin{pmatrix} \sin(\pi x_1)\cos(\pi x_2) + x_1 \\ -\sin(\pi x_2)\cos(\pi x_1) + x_2 \end{pmatrix} \tag{57}$$

which corresponds to Example 7 in [9]. We choose $\alpha = 2$, $\gamma = 2/3$, $\beta = 1$, and perform the same uniform h-refinements study as in Section 5.3, as well as h-adaptive refinements with element order $p = 3$. Fig. 6(a) shows that with uniform refinements, our numerical solution converges at the optimal rate. Note that the slope is -0.33, where the abscissa represents degrees of freedom, which scales as h^{-2}; in previous subsection, the abscissa is h^{-1}. Unlike [9], where solution converges up to a harmonic vector field, our solution converges in $\boldsymbol{L}^2$ norm by virtue of prescribing the circulation. Fig 6(a) also shows the error and residual for the adaptively refined meshes; the shown slope on that interval is -1.43, which is close to the theoretical value of -1.5 since we are using elements of order 3 [5]. The solution u_1 on the mesh after 4 adaptive refinements is shown in Fig. 6(b). The mesh keeps being refined near the singularity, as expected.

6 Conclusion

In this paper, we present a DPG method for the planar div-curl system. In a multiply-connected domain, additional circulation constraints must be imposed to guarantee well-posedness of the problem. We propose

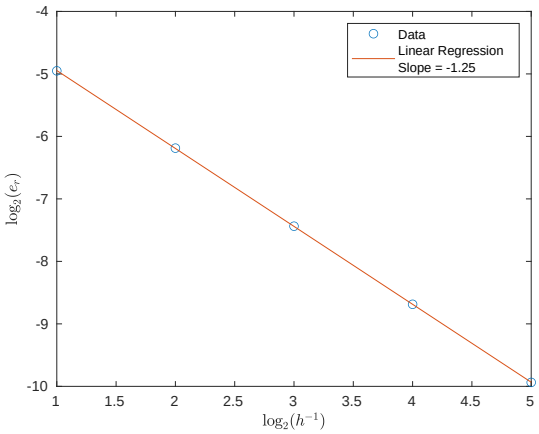

(a) $\gamma = 1.25$.

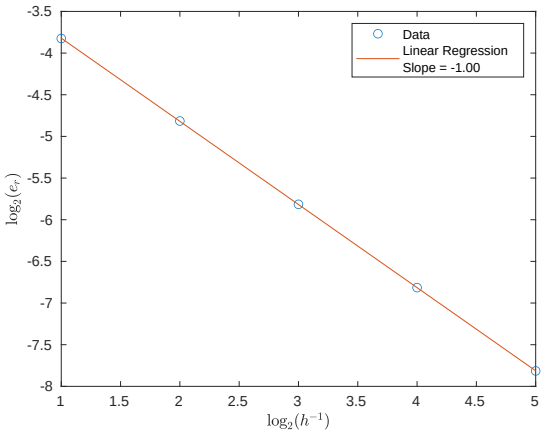

(b) $\gamma = 1$.

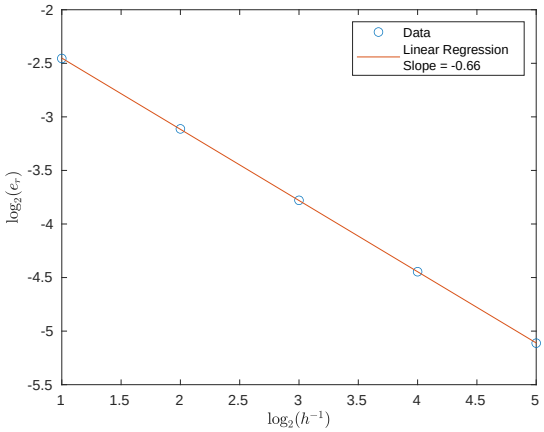

(c) $\gamma = 2/3$.

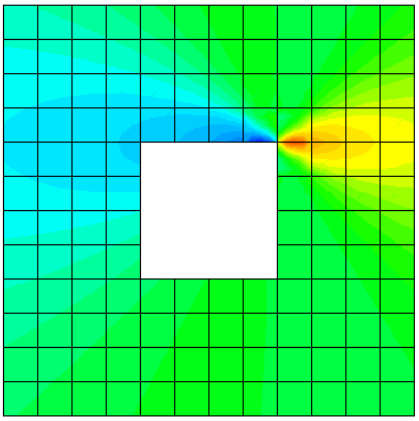

(d) Contour plot of u_1 for $\gamma = 2/3$ after 2 refinements, i.e. $h = 1/8$.

Figure 5: (a–c): Relative $\boldsymbol{L}^2$ error versus element size under uniform refinements. Blue circles represent errors in FE solutions, and red line is the linear regression line. (d): Contour plot of u_1.

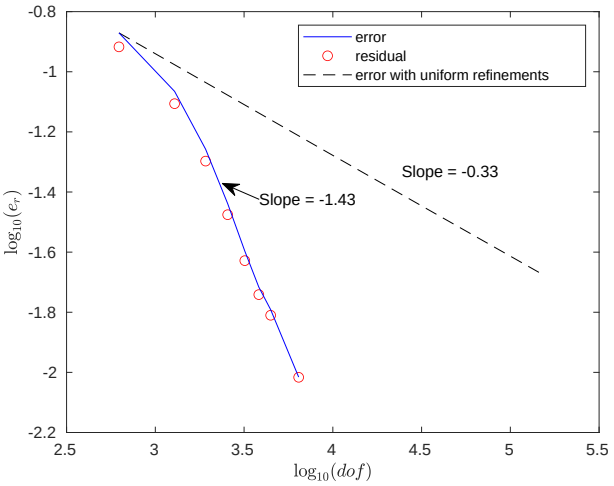

(a) Relative $\boldsymbol{L}^2$ error and residual versus degrees of freedom. The blue solid line represents relative error $\|\boldsymbol{u}-\boldsymbol{u}_h\|/\|\boldsymbol{u}\|$, red circles represent scaled residual $\|\boldsymbol{\psi}\|_{\mathcal{V}}/\|\boldsymbol{u}\|$, and the black dashed line stands for relative error with uniform refinements.

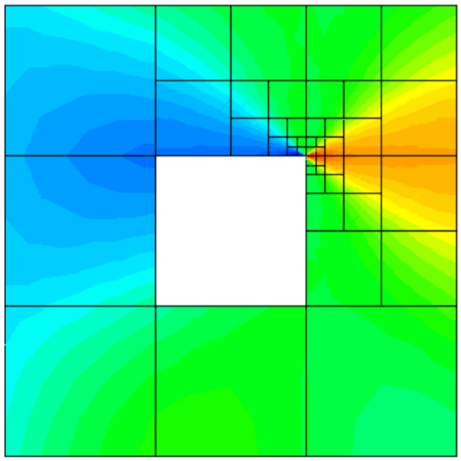

(b) Contour plot of u_1 on the adaptive mesh after 4 refinements.

Figure 6: Uniform and adaptive refinement study.

to impose the circulation constraint in a constrained minimization framework, and prove the discrete stability and convergence of our algorithm. Numerical experiments corroborate our analysis. Moreover, the DPG solution converges in L^2 norm at the optimal rate, not just asymptotically in the quotient norm. For singular problems, the adaptive solution is much better than that obtained on a uniform mesh.

Next step is the determination of the circulation, i.e., realizing Kutta condition in aerodynamics, for the flow around airfoil. We plan to use the postprocessing technique [4] to determine the circulation. This work will also lay the foundation for finite element solution of the full-potential equation [21], which can be viewed as a nonlinear div-curl problem.

Acknowledgements. This work is partly supported with NSF grant No. 1819101.

References

[1] J. D. Anderson. *Fundamentals of Aerodynamics*. 6th edition. New York, NY: McGraw Hill Education, 2017.

[2] G. Auchmuty. "Bounds and representations of solutions of planar div-curl problems". *Quarterly of Applied Mathematics* 75.3 (2017), pp. 505–524.

[3] G. Auchmuty and J. C. Alexander. "L^2 well-posedness of planar div-curl systems". *Archive for Rational Mechanics and Analysis* 160.2 (2001), pp. 91–134.

[4] I. Babuška and A. Miller. "The post-processing approach in the finite element method—Part 2: The calculation of stress intensity factors". *International Journal for Numerical Methods in Engineering* 20.6 (1984), pp. 1111–1129.

[5] I. Babuška, R. B. Kellogg, and J. Pitkäranta. "Direct and inverse error estimates for finite elements with mesh refinements". *Numerische Mathematik* 33.4 (1979), pp. 447–471.

[6] R. Bensow and M. G. Larson. "Discontinuous least-squares finite element method for the div-curl problem". *Numerische Mathematik* 101.4 (2005), pp. 601–617.

[7] P. B. Bochev, K. Peterson, and C. M. Siefert. "Analysis and computation of compatible least-squares methods for div-curl equations". *SIAM Journal on Numerical Analysis* 49.1 (2011), pp. 159–181.

[8] F. Brezzi. "On the existence, uniqueness and approximation of saddle-point problems arising from Lagrangian multipliers". *Publications mathématiques et informatique de Rennes* S4 (1974), pp. 1–26.

[9] S. Cao, C. Wang, and J. Wang. "A new numerical method for div-curl systems with low regularity assumptions". *Computers & Mathematics with Applications* 114 (2022), pp. 47–59.

[10] C. Carstensen, L. Demkowicz, and J. Gopalakrishnan. "Breaking spaces and forms for the DPG method and applications including Maxwell equations". *Computers & Mathematics with Applications* 72.3 (2016), pp. 494–522.

[11] C. Carstensen, L. Demkowicz, and J. Gopalakrishnan. "A posteriori error control for DPG methods". *SIAM Journal on Numerical Analysis* 52.3 (2014), pp. 1335–1353.

[12] J. Chan, L. Demkowicz, and R. Moser. "A DPG method for steady viscous compressible flow". *Computers & Fluids* 98 (2014), pp. 69–90.

[13] J. Chan et al. "A robust DPG method for convection-dominated diffusion problems II: Adjoint boundary conditions and mesh-dependent test norms". *Computers & Mathematics with Applications* 67.4 (2014), pp. 771–795.

[14] M. Costabel. "A coercive bilinear form for Maxwell's equations". *Journal of Mathematical Analysis and Applications* 157.2 (1991), pp. 527–541.

[15] L. Demkowicz and J. Gopalakrishnan. "A class of discontinuous Petrov-Galerkin methods. II. Optimal test functions". *Numerical Methods for Partial Differential Equations* 27.1 (2011), pp. 70–105.

[16] L. Demkowicz and J. Gopalakrishnan. "Encyclopedia of Computational Mechanics, Second Edition". Wiley, 2018. Chap. Discontinuous Petrov-Galerkin (DPG) Method.

[17] L. Demkowicz and P. Zanotti. "Construction of DPG Fortin operators revisited". *Computers & Mathematics with Applications* 80.11 (2020), pp. 2261–2271.

[18] L. F. Demkowicz, N. V. Roberts, and J. Muñoz-Matute. "The DPG Method for the Convection-Reaction Problem, Revisited". *Computational Methods in Applied Mathematics* (2022).

[19] T. Ellis, L. Demkowicz, and J. Chan. "Locally conservative discontinuous Petrov–Galerkin finite elements for fluid problems". *Computers & Mathematics with Applications* 68.11 (2014), pp. 1530–1549.

[20] A. Ern and J.-L. Guermond. *Theory and Practice of Finite Elements*. New York: Springer, 2004.

[21] M. Feistauer. *Mathematical Methods in Fluid Dynamics*. Chapman and Hall/CRC, 1993.

[22] F. Fuentes et al. "Orientation embedded high order shape functions for the exact sequence elements of all shapes". *Computers & Mathematics with Applications* 70.4 (2015), pp. 353–458.

[23] J. Gopalakrishnan and W. Qiu. "An analysis of the practical DPG method". *Mathematics of Computation* 83.286 (2013), pp. 537–552.

[24] J. M. Hyman and M. Shashkov. "Mimetic discretizations for Maxwell's equations". *Journal of Computational Physics* 151.2 (1999), pp. 881–909.

[25] B. Keith, F. Fuentes, and L. Demkowicz. "The DPG methodology applied to different variational formulations of linear elasticity". *Computer Methods in Applied Mechanics and Engineering* 309 (2016), pp. 579–609.

[26] B. Keith et al. "Discrete least-squares finite element methods". *Computer Methods in Applied Mechanics and Engineering* 327 (2017), pp. 226–255.

[27] J. Li and L. Demkowicz. "An L^p-DPG method for the convection–diffusion problem". *Computers & Mathematics with Applications* 95 (2021), pp. 172–185.

[28] J. Li and L. Demkowicz. "An L^p-DPG method with application to 2D convection-diffusion problems". *Computational Methods in Applied Mathematics* 22.3 (2022), pp. 649–662.

[29] I. Muga and K. G. Van Der Zee. "Discretization of linear problems in Banach spaces: residual minimization, nonlinear Petrov–Galerkin, and monotone mixed methods". *SIAM Journal on Numerical Analysis* 58.6 (2020), pp. 3406–3426.

[30] R. A. Nicolaides. "Direct discretization of planar div-curl problems". *SIAM Journal on Numerical Analysis* 29.1 (1992), pp. 32–56.

[31] R. A. Nicolaides and X. Wu. "Covolume solutions of three-dimensional div-curl equations". *SIAM Journal on Numerical Analysis* 34.6 (1997), pp. 2195–2203.

[32] J. T. Oden and L. Demkowicz. *Applied Functional Analysis*. Third edition. Boca Raton: CRC Press/Taylor & Franics Group, 2018.

[33] S. Petrides and L. F. Demkowicz. "An adaptive DPG method for high frequency time-harmonic wave propagation problems". *Computers & Mathematics with Applications* 74.8 (2017), pp. 1999–2017.

[34] W. Rachowicz, A. Zdunek, and W. Cecot. "A discontinuous Petrov-Galerkin method for compressible Navier-Stokes equations in three dimensions". *Computers & Mathematics with Applications* 102 (2021), pp. 113–136.

[35] N. V. Roberts, T. Bui-Thanh, and L. Demkowicz. "The DPG method for the Stokes problem". *Computers & Mathematics with Applications* 67.4 (2014), pp. 966–995.

[36] N. V. Roberts, L. Demkowicz, and R. Moser. "A discontinuous Petrov–Galerkin methodology for adaptive solutions to the incompressible Navier–Stokes equations". *Journal of Computational Physics* 301 (2015), pp. 456–483.

[37] J. Zitelli et al. "A class of discontinuous Petrov–Galerkin methods. Part IV: The optimal test norm and time-harmonic wave propagation in 1D". *Journal of Computational Physics* 230.7 (2011), pp. 2406–2432.